

# Forward-only learning in memristor arrays with month-scale stability

Adrien Renaudineau<sup>1</sup>, Mamadou Hawa Diallo<sup>2,+</sup>, Théo Dupuis<sup>1,+</sup>, Bastien Imbert<sup>2,+</sup>, Mohammed Akib Iftakher<sup>1</sup>, Kamel-Eddine Harabi<sup>3</sup>, Clément Turck<sup>1</sup>, Tifenn Hirtzlin<sup>3</sup>, Djohan Bonnet<sup>1</sup>, Franck Melul<sup>2</sup>, Jorge-Daniel Aguirre-Morales<sup>2</sup>, Elisa Vianello<sup>3</sup>, Marc Bocquet<sup>2</sup>, Jean-Michel Portal<sup>2</sup>, and Damien Querlioz<sup>1,\*</sup>

<sup>1</sup>Université Paris-Saclay, CNRS, Centre de Nanosciences et de Nanotechnologies, Palaiseau, France

<sup>2</sup>Aix-Marseille Université, CNRS, Institut Matériaux Microélectronique Nanosciences de Provence, Marseille, France

<sup>3</sup>Université Grenoble-Alpes, CEA, LETI, Grenoble, France

\*damien.querlioz@universite-paris-saclay.fr

+These authors contributed equally to this work

## ABSTRACT

Turning memristor arrays from efficient inference engines into systems capable of on-chip learning has proved difficult. Weight updates have a high energy cost and cause device wear, analog states drift, and backpropagation requires a backward pass with reversed signal flow. Here we experimentally demonstrate learning on standard filamentary  $\text{HfO}_x/\text{Ti}$  arrays that addresses these challenges with two design choices. First, we realize that standard filamentary  $\text{HfO}_x/\text{Ti}$  memristors support sub-1 V reset-only pulses that cut energy, improve endurance, and yield stable analog states. Second, we rely on forward-only training algorithms derived from Hinton's Forward-Forward that use only inference-style operations. We train two-layer classifiers on an ImageNet-resolution four-class task using arrays up to 8,064 devices. Two forward-only variants, the double-pass supervised Forward-Forward and a single-pass competitive rule, achieve test accuracies of 89.5% and 89.6%, respectively; a reference experiment using backpropagation reaches 90.0%. Across five independent runs per method, these accuracies match within statistical uncertainty. Trained models retain accuracy for at least one month under ambient conditions, consistent with the stability of reset-only states. Sub-1 V reset updates use 460 times less energy than conventional program-and-verify programming and require just 46% more energy than inference-only operation. Together, these results establish forward-only, sub-1 V learning on standard filamentary stacks at array scale, outlining a practical, pulse-aware route to adaptive edge intelligence.

## Introduction

Artificial synapses based on memristors perform analog multiply-accumulate (MAC) operations by Ohm's and Kirchhoff's laws, enabling remarkably low inference energy<sup>1–6</sup> (with closely related results using phase-change memory<sup>7,8</sup>). As large-scale memristor-based inference has now been demonstrated, the next frontier is on-chip learning. This capability is critical for edge scenarios, e.g., medical sensing or predictive maintenance, where models must adapt *in situ* to potentially confidential information.

However, learning in memory is far more demanding than inference, due to both device-level and algorithmic-level factors.

At the device level, training means many small weight changes. Analog programming of memristors typically uses long program-and-verify loops<sup>9,10</sup>: successive high-voltage pulses (bit-line higher than 1 V, i.e., above the nominal supply of advanced CMOS) are applied until a target conductance is reached, which costs energy and accelerates device wear. Devices engineered for incremental potentiation/depression can avoid program-and-verify<sup>11,12</sup>, but they generally still require bit-line voltages above one volt and trade learning capability for retention and stability. To sidestep these issues, some works learn in easier-to-write memories (SRAM<sup>13</sup> or ferroelectric capacitors<sup>14</sup>), and periodically transfer weights to memristors, at the price of considerable auxiliary memory. A more economical route is to learn directly in memristors. Here, we demonstrate a solution that relies on standard, industry-ready filamentary  $\text{HfO}_x/\text{Ti}$  memristors. We use a sub-1 V, reset-only training that reduces energy consumption, preserves endurance, and yields months-long post-training stability.

At the algorithmic level, backpropagation, the standard for training multilayer neural networks, uses different operations than inference: it needs a backward pass with transpose-array access and reversed signal flow, and storage of layer activations. Here, we instead adopt forward-only algorithms derived from the Forward-Forward framework proposed by Geoffrey Hinton<sup>15</sup>. In these algorithms, each layer optimizes a local “goodness” of its activations using the same MAC operations as inference, i.e., exactly the operation memristor arrays excel at doing. Specifically, we evaluate supervised Forward-Forward (SFF), which uses two forward passes and follows Hinton’s original proposal, and a competitive, cluster-based single-pass scheme inspired by<sup>16</sup>.

Combining these device-level and algorithmic choices, we experimentally train two-layer classifiers on an ImageNet-resolution four-class transfer task (bear species) using arrays up to 8,064 devices. All weight updates use identical sub-1 V, sign-only, thresholded pulses. Final test accuracies reach 89.5% (SFF) and 89.6% (competitive forward). Floating-point software backpropagation achieves 93.8%. We also include a backpropagation reference in which the backward pass is computed in software while all weight updates are executed on hardware with the same sub-1 V rule; this reference attains 90.0%. Across five independent runs per method, differences among SFF, competitive forward, and the backpropagation reference are not statistically significant.

Only a few experimental works have demonstrated full *in situ* learning directly on memristive hardware, using different strategies to approach the challenge of hardware backpropagation. Early experimental demonstrations of learning directly in memristors trained single-layer networks, which do not require backpropagation, for logic or small-pattern/face classification<sup>17-20</sup>. STELLAR avoided backpropagation by training only the second layer of a two-layer network<sup>21</sup>. Other studies used a software backward pass<sup>22</sup> or a Hopfield-type local activity-difference rule avoiding backpropagation but requiring iterative equilibria per input<sup>23</sup>. Ref.<sup>24</sup> implemented a backward pass in hardware but on a minimal XOR task using six nanodevices. None of these works examined post-training accuracy stability after on-chip learning. When multi-week retention is reported (e.g.,  $\sim$ 48 days in<sup>21</sup> or 30 days in<sup>9</sup>), it pertains to off-chip-trained weights written via program-and-verify. These gaps motivate the sub-1 V reset-only regime adopted here, targeting both safe operating voltages and post-training stability.

To the best of our knowledge, this Article presents the first array-scale demonstration of on-chip learning with sub-1 V reset-only updates, the first report of month-scale accuracy stability after on-chip training, and the first large-scale (up to 8,064 devices) Forward-Forward-type demonstration on memristors. Preliminary, simulation-based versions of parts of this work appeared in<sup>25</sup>; here we report the full experimental realization. These results chart a practical path from energy-efficient in-memory inference to on-chip learning using standard filamentary stacks operated safely below one volt.

## Results

### Sub-1 V memristor programming

Memristor arrays excel at analog inference, but on-chip learning requires repeated, fine-grained weight updates, making device programming variability and wear rate central constraints. In filamentary devices, the common approach is to program conductance by controlling the compliance current during the set operation and using program-and-verify loops<sup>9,10</sup>. This approach achieves precise targets but demands bit-line voltages exceeding 1 V and incurs multiple pulses per update, which is detrimental for device endurance. These conditions may be used in specially optimized few-shot learning contexts<sup>26</sup> but are incompatible with frequent learning steps.

We instead exploit progressive filament dissolution using low-amplitude reset pulses. Short sub-1 V pulses applied to the bit line partially erode the conductive filament and monotonically decrease conductance by small increments (Fig. 1b; device and characterization details are provided in Methods). Reset-only control is unidirectional. However, in nearly all memristor analog neural networks, each synaptic weight is encoded as a differential pair of conductances,  $w \propto G^+ - G^-$  (this technique allows implementing signed weights). Therefore, in our case, a positive weight update is implemented by slightly resetting the “negative” device, and a negative update by resetting the “positive” device (Fig. 1c). This scheme provides signed updates while keeping all programming, sub one-volt. Note that, throughout, “sub-1 V” denotes the memristor terminal voltage (bit line to source line,  $V_{BL} - V_{SL}$ ). In our 130-nm 1T1R arrays, we overdrive the word line ( $>1$  V) to reduce access resistance; this does not raise  $(V_{BL} - V_{SL})$ , which stays  $<1$  V during reset-only updates, and is unnecessary in advanced nodes (see Methods).

When training, to reduce energy and wear, and avoid the low-conductance regime where sub-1 V resets lose monotonicity, we restrict per-device updates with two rules. *Selective updates*: apply an update only when the gradient magnitude exceeds a threshold  $\tau$ . *Sign-only pulses*: when triggered, ignore the gradient magnitude and apply exactly one sub-1 V reset to the appropriate device of the differential pair (a positive gradient pulses the “negative” device; a negative gradient pulses the “positive” device).

Operating in the sub-1 V reset-only regime brings two benefits. First, endurance is promoted because each update uses a single, low-voltage pulse. We stressed four devices with 1.5 million 0.9 V resets, inserting a full reset/set reinitialization every 5,000 pulses to return to low resistance. The progressive resistance increase is preserved (Fig. 1d), which is the feature critical for learning. Notably, the memory window widens with cycling, consistent with a reset “wake-up” effect.

Second, retention is enhanced notably relative to states created by set with compliance current

programming: starting from a thick, stable filament (low-resistance state) and only partially dissolving it yields states that drift less over time. This high retention is seen in Fig. 1e. We programmed 3,456 devices to various conductances ranging between  $16 \mu\text{S}$  and  $100 \mu\text{S}$  and measured the drift in their conductance after 8, 20, and 90 days. Fig. 1e shows the cumulative probability distribution of the measured drift and confirms the high stability of the programmed states: 90.7% of devices have drifted by less than  $3 \mu\text{S}$  after 90 days. Suppl. Fig. 2 shows that the more conventional approach of programming by set under current compliance produces markedly higher drift within hours. The superior stability of reset-programmed analog states has also been observed using regular ( $>1 \text{ V}$ ) reset<sup>26,27</sup>.

These advantages come with characteristic non-idealities: Update magnitudes are stochastic from pulse to pulse due to the atomic-scale filament geometry and trap-assisted processes<sup>28</sup>. The effective analog memory window is also reduced compared with conventional program-and-verify: As the filament approaches full dissolution, a late-stage regime exhibits increased variability, which limits the practical number of reliable pulses between reinitializations.

Device-to-device dispersion is also significant; nevertheless, the progressive, mostly monotonic behavior is observed consistently in all of the measured devices. To characterize the quality of the sub-1 V reset regime of a particular device we compute the Pearson correlation coefficient between number of applied pulses and device conductance (see Methods). This coefficient measures how well the conductance vs. pulse number curve can be approximated by a straight line. Fig. 1f shows the distribution of the Pearson coefficient of 1,268 devices, and for select values, a random example of conductance vs. number of pulses curves. Most devices have a Pearson coefficient close to -1, indicating a nearly linear relationship between conductance and pulse number. However, a non-negligible subset deviates from this trend, with some devices showing Pearson coefficients near zero or even positive. In the next section, we assess experimentally the impact of these imperfect devices on learning.

The sub-1 V reset regime can be optimized to a certain extent. We find that several aspects of the sub-1 V reset-only response can be tuned through forming conditions (Supplementary Note 1). In summary, a single fixed bias-forming pulse followed by set-reset “wake-up” cycles establishes a progressive, approximately monotonic reset slope. Still, the response remains stochastic to a large extent. In the remainder of this Article, we design and evaluate learning procedures that are explicitly matched to these programming characteristics and demonstrate experimentally that they are sufficient for stable, large-scale training on memristor arrays.

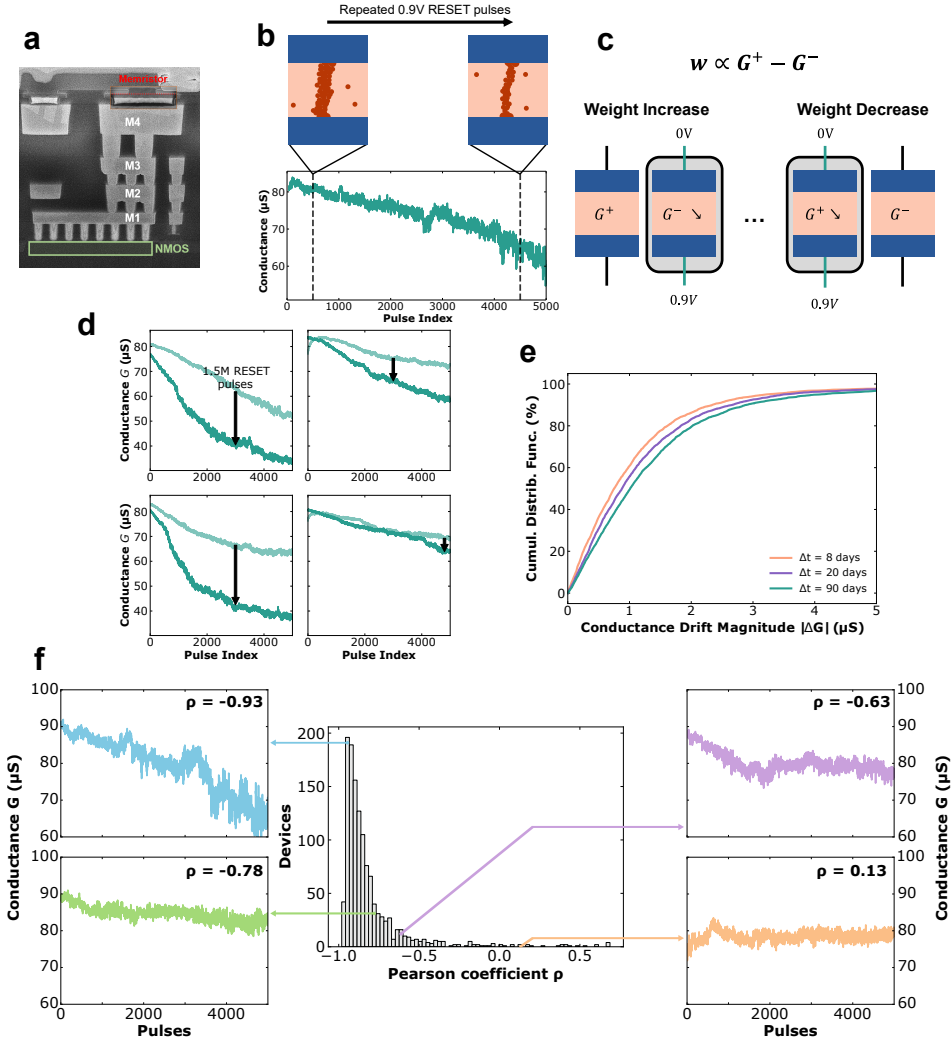


**Figure 1. Sub-1 V reset regime of  $\text{HfO}_x/\text{Ti}$  memristors.** **a** Focused ion beam-scanning electron microscopy (FIB-SEM) image of a cut circuit showing memristor integrated over CMOS. **b** Proposed low-voltage reset procedure: No conductance is targeted, only its progressive decrease via the partial dissolution of an existing filament via repeated, same-low-voltage pulses. **c** To both increase and decrease weights, as well as enabling negative values, memristors are in pairs. The difference of their conductance is encoding a single weight and therefore only one of the two have a low-voltage pulse applied to depending on the sign of the update. **d** Endurance of four devices programmed with sub-1 V reset: for each device, the dynamics over 5,000 pulses stays similar after 300 cycles and 1,500,000 pulses. The curves are averaged over the 20 first and 20 last cycles. **e** Retention of 3,456 devices programmed with sub-1 V reset: 8 days after training, 94.1% drifted by less than 3  $\mu$ S, and 90.7% after 90 days. **f** Distribution of the Pearson coefficient of conductance vs. pulse number curves for 1,268 memristors. Randomly-chosen examples of curves are presented for different Pearson coefficients.

## Backpropagation-based learning with sub-1 V memristor programming

We target an edge-learning setting in which a cloud-pretrained backbone is adapted *in situ* via transfer learning rather than trained end-to-end. Concretely, we take an ImageNet-pretrained network, remove its final classifier, and replace it with memristor-implemented layers retrained on device to specialize the model (Fig. 2a). In this proof-of-concept, the convolutional backbone is emulated in software. In a deployable system, it could be realized as an ultra-efficient fixed-weight front end that hardwires the convolutional synapses, trading programmability for extreme energy efficiency. Multiple demonstrations of such hardwired convolutional backbones have been demonstrated using register-transfer-level synthesis<sup>29</sup> or read-only memory<sup>30-32</sup>.

As a compact, ImageNet-resolution task, we classify four bear species (brown bear, sloth bear, polar bear, giant panda) using only a few thousand labeled images for fine-tuning (see Methods). The ImageNet-pretrained backbone yields a 512-dimensional feature vector at its penultimate layer. To match the input of our memristor arrays, reduce data movement, and keep the problem challenging for this proof-of-concept, we retain only the first 32 channels of this vector and train the memristor head on them. This 32-dimension input is used identically for train/validation/test across software baselines and hardware runs (see Methods; Supplementary Fig. 4 confirms that the 32-dimension task remains solvable but is harder than using the full 512 dimensions).

Before studying forward-only learning approaches, we first perform reference experiments using conventional, backpropagation-based learning. We consider single-layer (perceptron) and two-layer memristor classifiers. Figs. 2b,c shows the hybrid CMOS/memristor “MAC array” circuit that we use to train the perceptron. It features a  $32 \times 64$  memristor array that performs multiply-and-accumulate (MAC) operations in analog using Ohm’s and Kirchhoff’s laws (see Methods). In differential encoding, columns for  $G_{ij}^+$  and  $G_{ij}^-$  are driven by  $\pm x_j V_{read}$ . The column current for class  $i$  is therefore

$$I_i = \sum_j (G_{ij}^+ - G_{ij}^-) x_j V_{read}, \quad (1)$$

and logits are read as  $y_i = \kappa I_i$  with a fixed gain  $\kappa$ . Fig. 2d shows the measured output of the MAC array versus the expected software MAC, confirming high accuracy over a wide input/output range.

To perform a learning experiment, for each batch of data, we perform the forward pass experimentally, compute the gradients in software based on the results of the forward pass (see Methods) and then adjust the conductances based on the principles described in the previous paragraph. Experimentally (five independent runs), the perceptron reaches a mean final accuracy of 69.5% (Fig. 2e). The experiments have high variation as the accuracy ranged between 65.3 and 76.7% (the standard deviation is 4.3%).

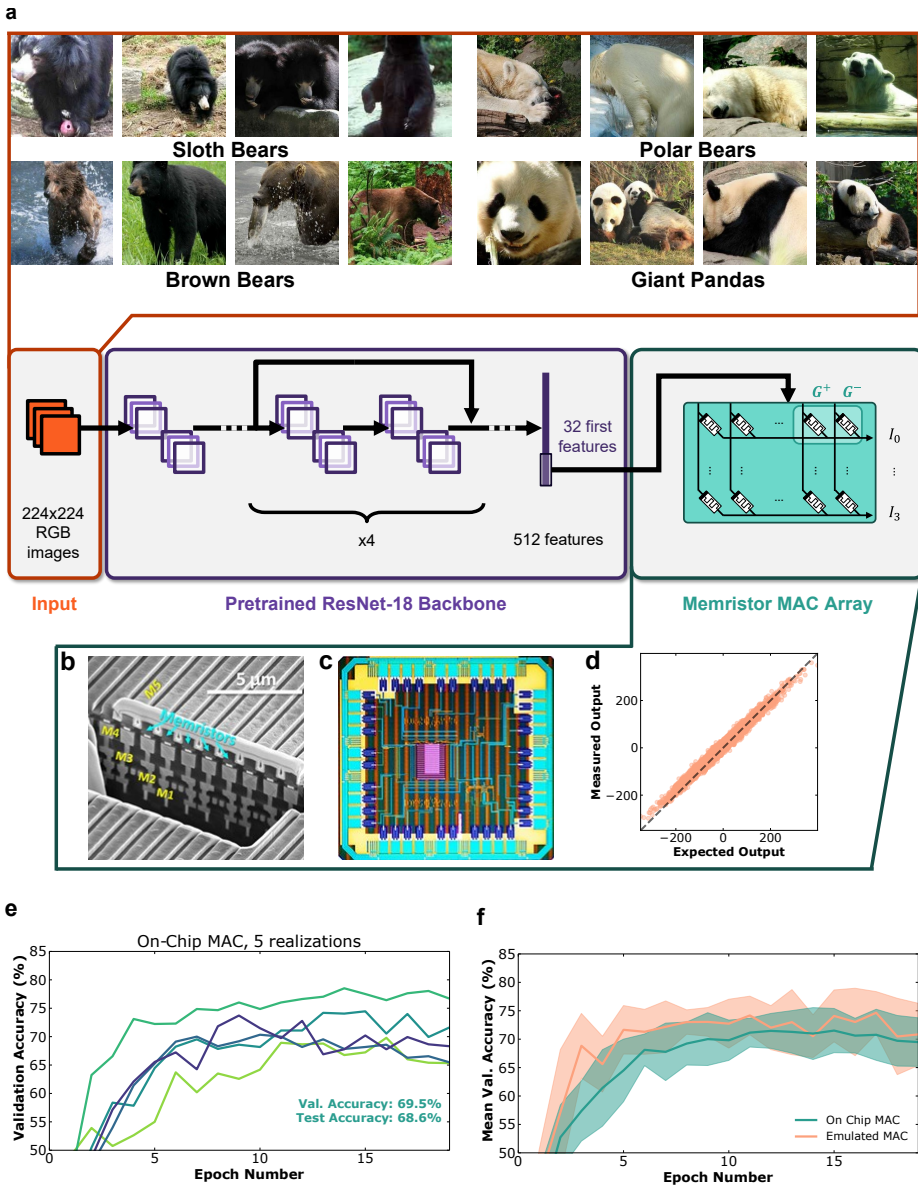


**Figure 2. Experimental transfer training of a memristor crossbar on bear classification using perceptron architecture.** **a** Topology of the trained architecture associating a ResNet pretrained on ImageNet with a memristor crossbar trained on bear species classification. **b** Focused ion beam-scanning electron microscopy (FIB-SEM) image of a memristor array integrated over CMOS. **c** Optical microscopy image of the multiply-and-accumulate (MAC) memristor/CMOS integrated circuit. **d** Experimental validation of the MAC functionality: measured output as a function of result expected from software MAC on a variety of inputs (see Methods). **e** Evolution of validation accuracy over five experimental realizations of the training. MAC operations as well as memristor updates are performed on-chip. **f** Comparison of the mean result of **e** with the mean results of five control experiments where only memristor updates are performed on-chip, and MACs are emulated by software to speed up experiments.

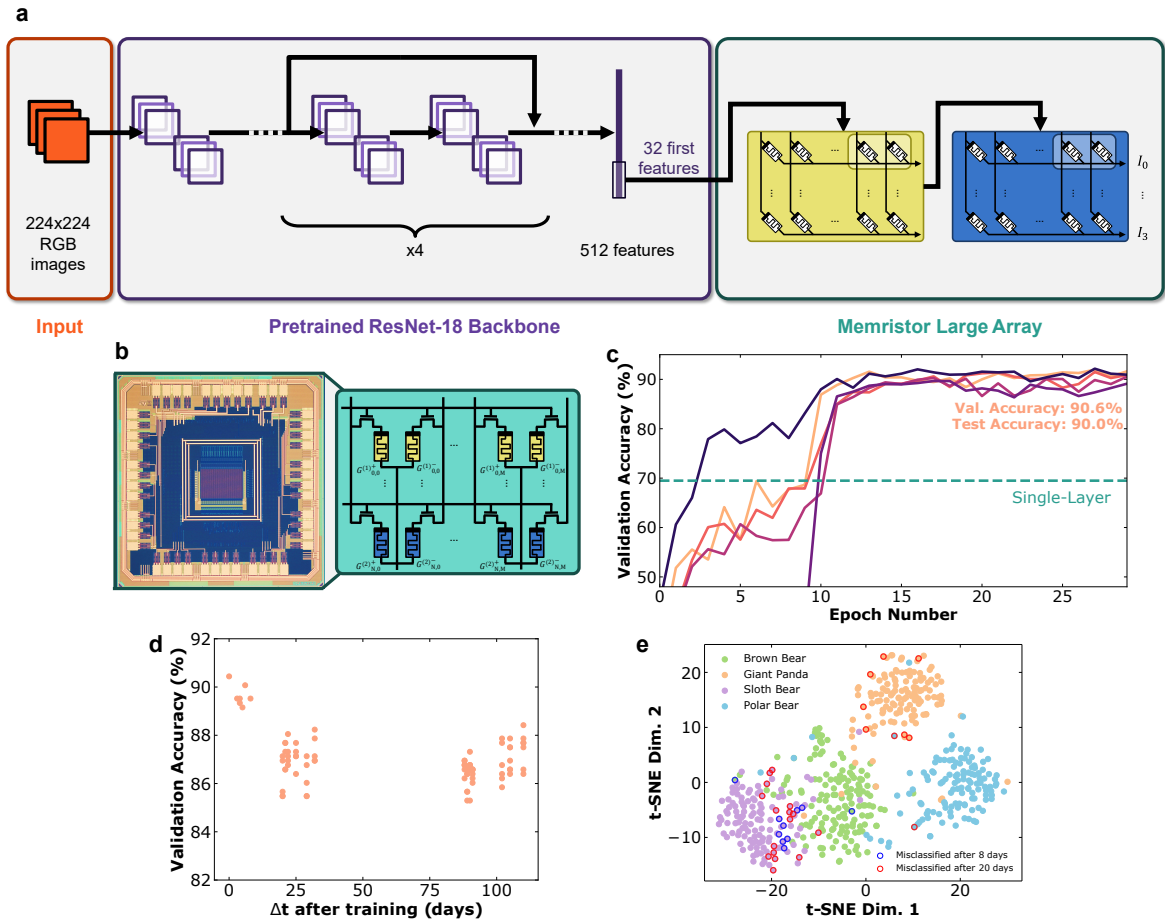


**Figure 3. Experimental transfer training of a memristor crossbar on bear classification using a multilayer perceptron architecture and backpropagation.** **a** Topology of the trained architecture associating a ResNet pretrained on ImageNet with two memristor crossbars. **b** Optical microscopy image and simplified schematic of the “large array” memristor/CMOS integrated circuit. **c** Evolution of validation accuracy over five experimental realizations of the training. All memristor updates are performed on-chip, MACs are emulated by software to speed up experiments (unlike Fig. 2 where they are performed on chip). **d** Evolution of the validation accuracy over time once training is finished for one circuit. **e** t-SNE representation of the bear test dataset. The samples initially classified correctly and then incorrectly after 8 and 20 days are marked.

For the two-layer network (Fig. 3a), we use the “Large Array,” a  $128 \times 64$  1T1R hybrid CMOS/memristor chip with direct analog device access but no on-chip MAC (Fig. 3b; Methods). To accelerate multilayer experiments, we adopt a hardware-in-the-loop protocol: MACs are emulated in software while all weight reads/writes occur on hardware. At each training step we (i) read all devices and map them to weights using  $W = s(G^+ - G^-)$ ; (ii) run batched inference and compute gradients in PyTorch; (iii) apply at most one sub-1 V reset to the appropriate device of each selected differential pair (sign-only, thresholded); (iv) re-read to refresh  $W$ . With this technique all device-level effects of the sub-1 V reset regime (stochastic step sizes, limited analog window, drift) are still done in hardware, while greatly reducing runtime. We verified on the perceptron that on-chip MAC and hardware-in-the-loop experiments yield matching learning curves and final accuracy (Fig. 2f).

We found when training multilayer classifiers that training all layers simultaneously, as is usually done in software, amplifies device noise and stochastic update variability (see Suppl. Fig. 5). We therefore adopted a layer-wise schedule: first train the layer closest to the output, then freeze it and train the preceding layer. This simple schedule consistently improved convergence under hardware non-idealities.

Experimentally, the two-layer network (multilayer perceptron, MLP) attains 90.0%, with markedly tighter standard deviation (1.1% over five runs) than in the perceptron case (Fig. 3c). For comparison, software baselines of perceptron and two layer neural network (same architecture, floating-point training) achieve 93.3% and 93.8%, respectively. The larger hardware-software gap for the perceptron is noteworthy: Despite its simplicity, the single layer is more sensitive to stochastic, unidirectional updates and device-to-device dispersion, whereas the hidden layer in the MLP provides representational redundancy that absorbs programming noise and limited analog dynamic range. This behavior underscores that learning dynamics under sub-1 V reset constraints differ from conventional floating-point training, as in software implementations, perceptrons typically show easier and more robust convergence than MLPs. The three percentage point gap in the MLP case is significant, but it is still appreciably low when considering the highly stochastic nature of the sub-1 V reset regime.

As expected from the characteristics of the sub-1 V reset, the trained neural network shows remarkably stable accuracy, with no significant degradation one week after training (Fig. 3d) and three percentage points after one and three months. This result mirrors the remarkable stability of sub-1 V-reset-programmed memristor states observed in Fig. 1e.

Fig. 3e investigates which are the few bear samples that become misclassified after 8, 20, or 90 days although they were correctly classified after training. For this purpose, we plotted a t-distributed stochastic neighbor embedding (t-SNE) representation of our test dataset (see Methods), and we marked the samples that became misclassified in time. We observe that these few samples typically lie on the edges of the t-SNE blobs representing the different bear species. This observation suggests that they are edge, harder-to-classify samples. A similar observation has been made in the literature when looking at errors on a poorly illuminated, solar-powered near-memory-computing circuit<sup>33</sup>.

### Forward-pass-only learning with sub-1 V memristor programming

In the multilayer backpropagation experiments reported in the previous section, all array write operations are performed on hardware, while the surrounding control is emulated. Building a fully integrated

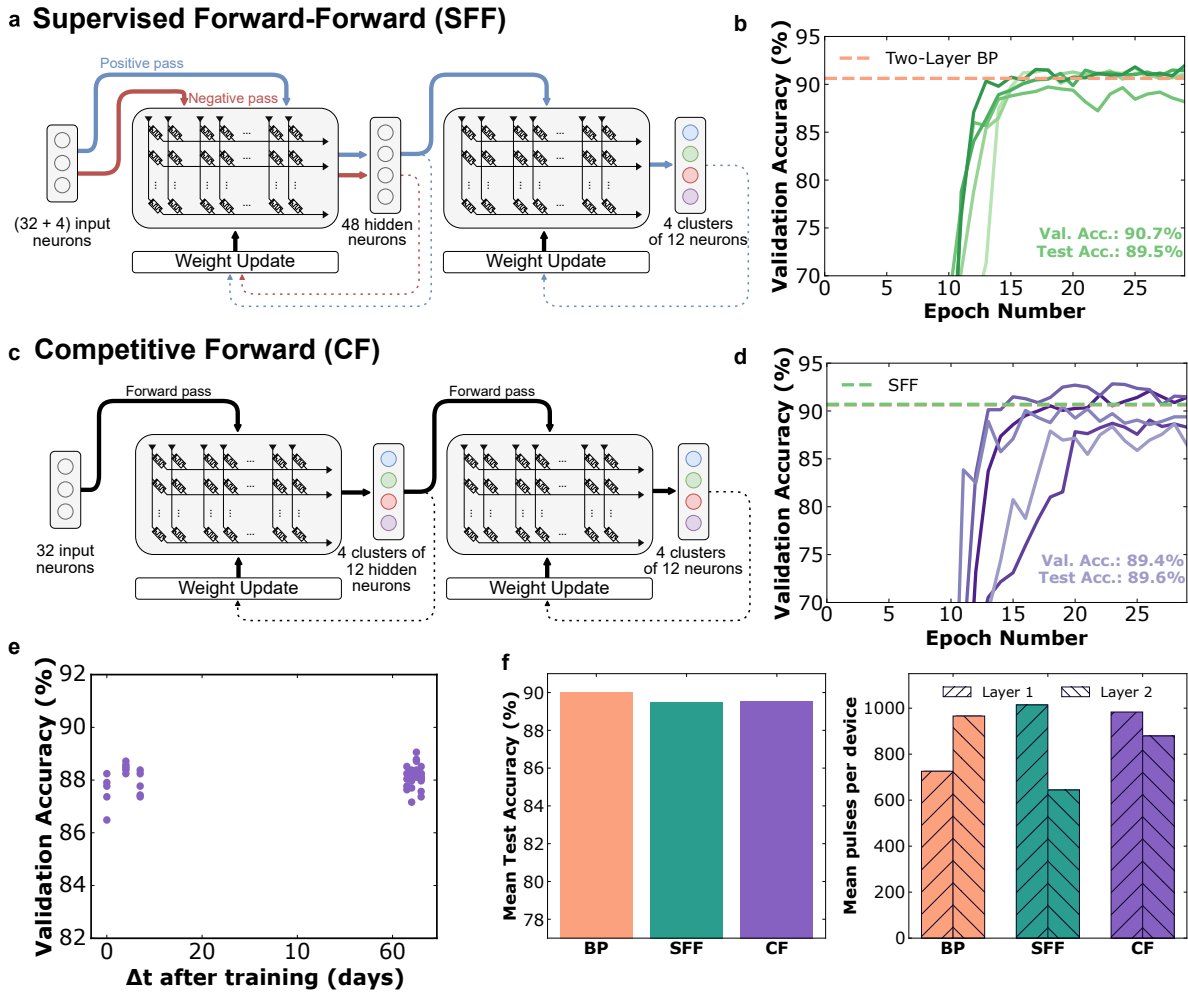


**Figure 4. Experimental transfer training of a memristor crossbar on bear classification using forward-only training approaches.** **a** Illustration of our Forward-Forward approach using “positive” and “negative” examples and a second memristor layer with competitive clusters. **b** Evolution of validation accuracy on bear classification over five experimental realizations of Forward-Forward training. Methodology for experiments is the same as Fig. 3. **c** Illustration of our competitive forward approach using two memristor layers with competitive clusters. **d** Evolution of validation accuracy on bear classification over five experimental realizations of competitive forward training. **e** Evolution of the validation accuracy over time once training is finished for one circuit trained with competitive forward. **f** Comparison of mean test accuracy, and mean number of sub-1 V reset pulses per device in our experiments employing backpropagation, Forward-Forward, and competitive forward training.

system around backpropagation, however, is challenging: it requires a backward pass (transpose-array access or weight reuse with reversing signal flow), storage of layer activations, and additional on-chip compute, which together impose substantial circuit and energy overhead. These challenges motivate forward-pass-only alternatives that avoid any backward signals.

We therefore evaluate two hardware-friendly schemes. The first is Hinton’s Forward-Forward algorithm<sup>15</sup>. Each layer computes a scalar “goodness” of its activations, which is the sum of the squared

activations of its neurons (see Methods). Training uses only forward passes on positive (data paired with the true label token) and negative (data paired with an incorrect label token) examples to maximize goodness on positives and minimize it on negatives. This is easily achieved using local weight updates requiring no backpropagated errors (see Methods, eq. (5)).

For readout, Hinton recommends using a large softmax head to extract output, spanning over several neural network layers, but this approach is poorly matched to sub-1 V reset. As shown earlier, shallow readouts degrade under hardware non-idealities. Second, it would require storing the activations of several layers, making it complicated to operate learning in a pipelined fashion (i.e., present a new input at the first layer, while the previous input is processed on the second layer).

To replace this softmax head, we use a memristor array acting as a bank of clusters (prototypes), one per class, each with 12 neurons (Fig. 4a). The idea is that during training, we aim at maximizing the goodness of the target cluster and minimizing the goodness of the other clusters. Conveniently, we can use the same goodness definition as the first layer, and the same local rule (see Methods, eq. (9)).

We implement Forward-Forward on memristor arrays using the same sub-1 V, sign-only, selective update rule as above and train layers sequentially. Unlike in the backpropagation case, we start training from the input side: As information is transmitted only in the forward direction in the Forward-Forward algorithm, no other sequence is possible. Experimentally (five runs), supervised Forward-Forward achieves a mean test accuracy of 89.5% (the standard deviation over five runs is 1.4%), within experimental uncertainty of the two-layer backpropagation baseline (90.0% with 1.1% standard deviation, Fig. 4b). In floating-point software, the two methods likewise match ( $\sim 93.8\%$ ). Consistent with this parity, the mean pulse count per device is similar across supervised Forward-Forward and backpropagation. However, the layer-wise distribution differs: in backpropagation the second (output) layer accumulates the most pulses, whereas in supervised Forward-Forward the first (input) layer does so (Fig. 4f). This inversion follows directly from the training schedules: backpropagation trains layers from output to input, supervised Forward-Forward from input to output, so in both cases the layer trained first receives the largest share of updates, while the second-trained layer primarily fine-tunes the network.

An important challenge with supervised Forward-Forward is the need to build positive and negative training examples, and the cost to perform two corresponding forward passes. To mitigate this issue, we built a network by stacking two cluster-based layers, similar to the one we use for readout in our supervised Forward-Forward experiments: we obtain what we call competitive forward (CF) learning, a purely forward, single-pass scheme built from stacked, all-to-all cluster layers (Fig. 4c). Each layer learns a set of competing prototypes; with depth, prototypes become more selective, and the final layer's clusters correspond to classes. Updates are local, use the same goodness equation as in supervised Forward-Forward, and the same selective, sign-only, single-pulse rule as in our other experiments, and layers are trained sequentially from input to output. The name “competitive forward” comes from the work of ref.<sup>16</sup>, which proposes a similar approach in software. However, whereas ref.<sup>16</sup> instantiates competitive clusters on the convolutional feature maps solely, we instead implement them as fully connected classifier heads, avoiding large softmax heads and aligning naturally with 1T1R crossbar topology and sub-1 V reset constraints.

As with supervised Forward-Forward, we train competitive forward layer by layer from input to

output (see Methods). Note that we inverted the sign of the goodness of the first layer (see Methods): this way, the first layer is driven to decrease the activity of the target cluster and increase the activity of the complementary clusters; the output layer then concentrates activity on the correct class. This sign asymmetry was not beneficial in floating-point software, but on hardware it reduces the pulse burden on the first layer (the one trained first), helping to avoid late-stage variability under sub-1 V reset and yielding more stable convergence.

Fig. 4d shows that across five experiments, competitive forward learning matches supervised Forward-Forward performance (mean test accuracy of 89.6%, with a standard deviation over five runs of 1.8%). A statistical test (see Methods) shows the difference in test accuracy observed between our experimental realization of competitive forward, supervised Forward-Forward, and the backpropagation experiments are not statistically significant, suggesting that the forward-only approaches are an excellent hardware-friendly alternative to backpropagation for the transfer learning task investigated here.

The mean number of pulses per device is similar between competitive forward and supervised Forward-Forward (Fig. 4f), with values around or below 1,000. Considering that we have demonstrated endurance of at least 1.5M pulses (Fig. 1d), this result means that the learning process can be repeated more than 1,500 times using the same memristor array.

Finally, Fig. 4e shows that the accuracy of a network trained by competitive forward is highly stable over two months. Unlike in the backpropagation case (Fig. 3e), no accuracy drop is seen (note that this experiment is performed with a network with an initial accuracy of 88%, i.e. lower than average). We attribute this even higher stability to the larger size of the forward-only network, and in particular, the final layer naturally features more redundancy than in the backpropagation case due to its cluster nature.

In the competitive-forward experiments on the large array, each programming pulse consumed 35 pJ on average. With the MAC-array, which uses devices optimized for lower-voltage operation, the per-pulse energy drops to 0.84 pJ; by contrast, a program-and-verify baseline requires 387 pJ per update (see Methods). Thus, optimized devices reduce energy by 42 relative to the large array conditions and by 460 relative to program-and-verify. Aggregated over the full competitive-forward run, resets consumed 251  $\mu$ J in our experiments; the same pulse counts on the optimized devices would total 6.0  $\mu$ J (see Methods).

Our lab-bench reads used 15  $\mu$ s integrations, which would lead to 21 mJ of read energy for the competitive-forward run. In a fully integrated implementation in an advanced CMOS node with faster sensing, these overheads should be far lower. Using the efficiency reported in ref.<sup>34</sup>, executing all MACs (including ADC) for the run would consume 13  $\mu$ J (see Methods), which is twice higher than the energy of sub-1 V reset pulses with the optimized devices: because sub-1 V resets are so inexpensive, implementing competitive-forward in hardware only adds modest overhead relative to inference-only designs. These extremely low-energy budgets are compatible with stringent edge power budgets.

## Discussion

Our experiments establish that on-chip learning is viable with sub-1 V reset programming of standard filamentary memristors. Competitive forward learning stands out as the most hardware-friendly

approach, in terms of implementation and it leads to accuracy on par with backpropagation on our bear classification example. It also shows month-long accuracy stability, even higher than the already high accuracy of the backpropagation trained neural network, as competitive forward learning uses a second layer with more redundancy than backpropagation.

The experimental demonstrations presented in this Article target an ImageNet-resolution, four-class bear task. To assess generality and enable ablations that would be impractical on hardware, we also used device-calibrated simulations that replay measured sub-1 V reset trajectories from 1,268 devices: each synaptic weight is mapped to a differential pair, and a sign-only update advances exactly one pulse along the recorded trace, reproducing stochastic step sizes without parametric fitting. On the bear task, these simulations closely map the hardware learning curves and final accuracies (Supplementary Note 3), supporting their use as a faithful proxy. In most cases experiments slightly outperform the device-calibrated simulations (Suppl. Table 3), which we attribute to the simulator’s finite pool of measured trajectories. Some traces must be reused across multiple simulated synapses, yielding a pessimistic estimate. Using the same simulator on the standard handwritten digit classification dataset MNIST (Supplementary Note 4), we observe qualitatively similar behavior and a comparable, modest gap to floating-point software: layer-wise backpropagation, supervised Forward-Forward, and competitive forward all perform well, with competitive forward consistently edging supervised Forward-Forward while retaining a single forward pass.

A central takeaway is that the learning dynamics under low-voltage reset differ materially from conventional software training. Unidirectional, stochastic, pulse-quantized updates and a limited analog window shift the optimization objective from “precise gradient following” toward “minimizing effective pulse usage while preserving useful signal”. In practice, this leads to design choices that are uncommon in software: selective (thresholded) updates, layer-wise training schedules, and classifier heads that offer representational redundancy (e.g., cluster layers) to absorb device variability. This last result corroborates with neuroscience simulations showing that redundancy allows reaching performances on par with reconfigurability of synaptic connections<sup>35</sup>, which is non-trivial in silicon hardware. Furthermore, because of the sub-1 V reset-only scheme, we use one-bit (sign-only) updates. Although motivated by hardware considerations, our approach is reminiscent of the “signSGD” optimizer introduced in software contexts<sup>36</sup>. Interestingly, to some extent, this optimizer appears as a special case of the Adam optimizer. Typically, Adam relies on first  $m_t$  and second  $v_t$  moments of the gradient  $g_t$ , for an update  $\propto m_t/\sqrt{v_t}$ . However, without momentum we have  $m_t = g_t$  and  $v_t = g_t^2$ , therefore  $m_t/\sqrt{v_t} = g_t/\sqrt{g_t^2} = \text{sgn}(g_t)$ . This optimizer can outperform the regular Adam in some scenarios<sup>37,38</sup>.

These choices reduce energy consumption and device wear and keep devices out of the late, high-variability dissolution regime. They also motivate pulse-aware training rules: regularize update counts, cap per-weight pulse budgets, and control update probability rather than amplitude. This algorithm-device co-design departs from standard learning-rate/weight-decay tuning and matches the quantized, unidirectional, stochastic nature of sub-1 V resets.

Our experiments use small minibatches (size 16) to stabilize updates. Because SFF and competitive-forward rules are local and we train layers sequentially, minibatching is much simpler than in backpropagation: to compute a layer’s weight updates, we only need that layer’s pre- and post-synaptic activations ( $x_\ell$  and  $h_\ell$ ). In practice, we buffer  $x_\ell$  and  $h_\ell$  for the 16 samples in a small working memory,

accumulate sufficient statistics over the batch, and then apply the sign-only updates (see Methods, eqs. (5) and (9)). The required memory is moderate as it scales with the number of neurons per layer, rather than the number of synapses as other works using auxiliary memory<sup>13, 14</sup>. Supplementary Note 3 analyzes batch-size trade-offs, indicating that micro-batches (size smaller than 16) recover most of the stability benefits while further reducing storage.

At the device level, the sub-1 V reset-only regime already delivers multiple advantages: safe sub-1 V operation, fewer pulses per update, improved endurance, and superior retention relative to set+compliance states. The remaining stochasticity, however, explains the few-percentage-point gap between multilayer hardware and software baselines, and the larger gap for single-layer perceptrons. Materials and stack engineering aimed at stabilizing filament geometry and trap landscapes, as well as pulse-shape optimization and modest circuit-level redundancy (e.g., small ensembles per weight or read averaging), are promising paths to close this gap without sacrificing the benefits of low-voltage operation.

Overall, our results chart a concrete route to practical, energy-efficient on-chip learning: adopt low-voltage reset programming; embrace pulse-aware, forward-leaning training rules that minimize updates; and provision minimal, local working memory where needed. With continued co-optimization across devices, circuits, and algorithms, including hybrid near-array memories and pulse-budgeted learning rules, the accuracy-energy envelope of sub-1 V memristor learning should improve further, enabling adaptive edge intelligence beyond the inference-only regime.

## Acknowledgements

This work benefited from France 2030 government grants managed by the French National Research Agency (ANR-22-PEEL-0010, ANR-22-PEEL-0013, ANR-23-PEIA-0002). The authors would like to thank Olivier Faure, Julie Grollier, Louis Hutin, Jonathan Miquel, and David Novo for discussion and invaluable feedback. A large language model (OpenAI ChatGPT) was used for copyediting parts of this manuscript.

## Author contributions statement

A.R. developed the code base of the project and performed the learning experiments, with assistance from M.A.I. M.H.D. proposed and developed the hardware adaptions of the Forward-Forward algorithms with J.D.A.-M. and F.M. T.D. proposed cluster-based forward-only learning and performed all bear-dataset and MNIST simulations. B.I. performed the preparatory simulations for hardware Forward-Forward algorithms. A.R. and T.H. developed the initial backpropagation study. D.B., A.R., and T.D. curated the bears dataset. K.E.H. designed the hybrid CMOS/memristor test chip. E.V. led the fabrication of the hybrid CMOS/memristor test chip. C.T. designed the test setup and its printed circuit board. J.M.P., M. B, and D.Q. supervised the work. D.Q. wrote the initial version of the manuscript. All authors discussed the results and reviewed the manuscript.

## Competing interests

The authors declare no competing interests.

## Data availability

The data measured in this study are available from the corresponding author upon request.

## Code availability

The software programs developed for this work are available online: <https://github.com/INTEGNANO/ForwardLearningUnderOneVolt>.

## Methods

### Design and fabrication of hybrid memristor/CMOS circuits

The hybrid circuits were produced in three stages, building on prior integration work<sup>33,39,40</sup>. In the first stage, the complementary metal-oxide-semiconductor (CMOS) front end was manufactured at a commercial foundry using a 130-nm low-power technology node with four metal interconnect layers. The second stage involved the integration of hafnium oxide  $\text{HfO}_x$  memristive devices on top of the fourth metal layer. Each device exhibits a stacked configuration consisting of titanium nitride (TiN),  $\text{HfO}_x$ , titanium (Ti), and a top TiN electrode. The  $\text{HfO}_x$  functional layer was deposited by atomic layer deposition (ALD). Device patterning defined a circular geometry with a 300-nm diameter. Following this integration, a fifth metal interconnect layer was deposited above the memristor structures. In the final stage, the processed wafers were packaged into J-leaded Ceramic Chip Carrier (JLCC) modules by a commercial vendor.

Two memristor platforms were used:

- **MAC array (Figs. 2b-d).** This integrated circuit targets in-memory multiply-accumulate (MAC) operations. It contains a  $32 \times 64$  two-transistor-one-resistor (2T1R) array; each cell integrates one memristor and two access transistors that enable (i) per-device forming, set, reset, and read via “vertical” selection and (ii) column-wise MAC via “horizontal” selection. Peripheral circuits provide the required biasing and current readout for column accumulation. Because synaptic weights are encoded as differential conductance pairs, the 2,048 devices implement up to 1,024 synapses.
- **Large Array (Fig. 3b).** This integrated circuit is a conventional  $128 \times 64$  one-transistor-one-resistor (1T1R) array with source lines shared by adjacent cells. Its periphery supports both digital and analog access<sup>41</sup>; in this work we use only direct analog device access for reading and programming. With differential pairing, the 8,192 devices implement up to 4,096 synapses.

The two platforms were fabricated on different wafers. The MAC array uses a newer generation of the  $\text{HfO}_x$  integration flow optimized for lower-voltage programming.

### Sub-1 V reset regime characterization

We first characterized the sub-1 V reset regime on the Large Array (Fig. 1). Supplementary Note 1 details the rationale behind our forming strategy. Devices were formed using a constant-amplitude scheme: identical pulses were applied repetitively (one to five shots) until conduction appeared, rather

than using a voltage ramp. To reinforce a thick, stable filament, three wakeup reset-set pairs were then applied. We subsequently recorded conductance trajectories under long sequences of low-amplitude reset pulses (5,000 shots).

After a coarse sweep of pulse amplitude and width, we acquired fine-grained trajectories by applying 5,000 reset pulses at 0.9 V and 600 ns duration on a cohort of 1,268 devices. For each device, we quantified monotonicity/linearity of conductance change versus pulse count using a Pearson correlation coefficient between  $G_i$  (post- $i$ -th-pulse conductance) and the pulse index  $i$  over the first  $P_{\max}$  pulses:

$$\rho_G = \frac{1}{P_{\max}} \sum_{i=1}^{P_{\max}} \frac{(G_i - \mu_G)(i - (P_{\max} + 1)/2)}{\sigma_G \sigma_P}, \quad (2)$$

where  $\mu_G$  and  $\sigma_G$  are the mean and standard deviation over the considered pulse range, and  $\sigma_P$  is a normalizing constant:  $\sqrt{\sum_i (i - (P_{\max} + 1)/2)^2 / P_{\max}}$ . Values of the Pearson coefficient near  $-1$  indicate a nearly linear, strictly decreasing conductance with pulse number. The distribution of Pearson coefficients as well as sample conductance trajectories are presented in Fig. 1f.

We also assessed endurance by repeating 300 cycles of 5,000 reset pulses at 0.9 V on four devices (Fig. 1d). At the end of each of the 300 cycles, the devices were reinitialized using a high voltage reset and a set operation.

To assess retention of states created by sub-1 V reset, we initialized devices to a low-resistance state and then used only low-amplitude reset pulses to program 3,456 devices to conductances spanning 16-100  $\mu$ S. Devices were stored under ambient laboratory conditions (23°C) with no bias applied between measurements. Conductance was read at  $t = 8, 20$ , and 90 days using the same read conditions employed elsewhere. Drift was defined as  $\Delta G(t) = G(t) - G(0)$ , and we report the distribution of  $|\Delta G|$  across the population in Fig. 1e.

We re-optimized the programming conditions to reproduce comparable sub-1 V reset behavior on the MAC array, which uses a newer, lower-voltage device flow. On this platform we employed a single wake-up (reset-set reinforcement) cycle instead of three during forming, and used 0.62 V, 30 ns reset pulses for low-voltage updates. All read/program conditions for both platforms are listed in Supplementary Note 2. Note that all “sub-1 V” statements in this work refer to the voltage across the memristor terminals ( $V_{BL} - V_{SL}$ ). To fully turn on the access transistors in the 130-nm arrays and reduce series resistance during reads/programs, the word lines are driven with a boosted gate voltage  $> 1$  V. This word-line overdrive is confined to the transistor gate; the memristor terminal voltage during reset-only updates remains below 1 V. This separation improves read accuracy and programming reproducibility without altering the device stress conditions, and would not be necessary in an advanced CMOS node.

### Curation of the animal dataset

We constructed a four-class dataset (brown bear, sloth bear, polar bear, giant panda) from a subset of ImageNet-1k images<sup>42</sup>. After shuffling, images were split in a class-balanced manner into train (60%,  $\sim 800$  per class), validation (30%,  $\sim 370$  per class), and test (10%,  $\sim 135$  per class) sets. The training split was augmented to 1,000 images per class using standard transforms (random horizontal flip, color

jitter, and small rotations). All images were preprocessed to match the backbone (ResNet-18) input requirements (resize/crop and normalization consistent with ImageNet pretraining). Supplementary Fig. 3 shows sample images of the dataset.

For all simulations and hardware experiments, we removed the backbone’s final classifier and extracted the 512-dimensional penultimate feature vector for each image. To emulate resource-constrained edge settings and reduce I/O, as well as make the classification task more challenging, we then restricted the feature space to 32 dimensions by retaining the first 32 channels of the 512-D vector (the same fixed subset for train/validation/test). The resulting 32-D features were cached and used identically across software baselines and on-chip experiments. Supplementary Fig. 4 shows the t-SNE representation of the full 512-D dataset and the restricted 32-D version, confirming that the 32-D version is a harder classification task.

## Experimental Setup

Both integrated circuits were mounted on in-house printed circuit boards (PCBs) and driven by an STM32F746ZG microcontroller, which generated array-specific digital control (addressing, mode selection, timing). Read/write biasing and electrical measurements were provided by a Keysight B1530A Waveform Generator/Fast Measurement Unit (WGFMU). A host computer coordinated the MCU and WGFMU; experiments were scripted in Python (PyTorch) with a lightweight wrapper that abstracts the matrix-vector multiplications between the operation on the MAC array and the emulation for the Large Array.

### Learning experiments with the MAC array (Fig. 2)

The MAC array supports on-chip analog MAC and was used for the perceptron experiments (32 inputs, 4 outputs) of Fig. 2. To match the array’s three-level input interface, features were ternarized to  $x_j \in \{-1, 0, +1\}$ . Simulations confirmed no measurable accuracy loss versus floating-point inputs for the bear-classification task, owing to the redundancy of the feature extractor.

**Biasing.** A differential weight is encoded as  $w_{ij} \propto G_{ij}^+ - G_{ij}^-$  using a pair of devices on adjacent columns. During inference, columns associated with  $G^+$  and  $G^-$  receive  $+x_j$  and  $-x_j$ , respectively. Negative input levels are synthesized by offsetting the source line (sense node) to  $V^0 = 0.7$  V and driving the bit lines at  $V^- = 0.5$  V,  $V^0$ , or  $V^+ = 0.9$  V for input levels  $x_j \in \{-1, 0, +1\}$ , yielding effective input voltages  $V_j^{\text{in}} \in \{-0.2, 0, +0.2\}$  V at the device.  $V^+$  is supplied by a DC source, while  $V^-$  and  $V^0$  are generated by the WGFMU.

**On-chip MAC and readout.** Let  $I_i$  be the column-summed current on output  $i$ . In differential encoding, columns for  $G_{ij}^+$  and  $G_{ij}^-$  are driven by  $\pm x_j V_{\text{read}}$ . The column current for class  $i$  is therefore

$$I_i = \sum_j (G_{ij}^+ x_j V_{\text{read}} + G_{ij}^- (-x_j) V_{\text{read}}) = \sum_j (G_{ij}^+ - G_{ij}^-) x_j V_{\text{read}}.$$

A scalar gain  $\kappa$  (software hyperparameter) maps  $I_i$  to the perceptron logits  $y_i = \kappa I_i$ .

**Row sequencing and software wrapper.** Because the WGFMU channel count limits simultaneous drive/sense, MAC is executed row-by-row. A custom PyTorch module wraps the hardware calls and

presents a `torch.nn.Linear`-like interface, configuring inputs and sequentially accumulating the on-chip MAC to form the output tensor. Training/validation/test metrics are thus computed with the same on-chip MAC path.

**Training loop.** Each update step consists of: (i) hardware forward pass on a mini-batch to obtain  $\mathbf{y}$ ; (ii) gradient computation; (iii) thresholding small gradients to zero (see Main text); and (iv) a programming sweep applying a single sub-1 V reset pulse to the appropriate device of each differential pair (pulse on  $G^-$  for a positive gradient, pulse on  $G^+$  for a negative gradient). A subsequent read sweep acquires  $G^+, G^-$  for logging and diagnostics.

#### **Learning experiments with the Large Array (Figs. 3 and 4)**

Because the MAC array is limited to  $32 \times 64$  devices, multilayer backpropagation and all forward-only experiments were performed on the Large Array ( $128 \times 64$ ). This platform does not implement on-chip MAC; instead, MAC operations are emulated in software while all weight reads/writes are executed on hardware. The equivalence of on-chip versus software MAC was verified on the perceptron using the MAC array (see Fig. 2f).

**Weight mapping.** After each hardware read, software weights are reconstructed from device conductances via a fixed scale factor  $s$ :

$$W = s (G^+ - G^-),$$

with  $(G^+, G^-)$  the differential pair assigned to each synapse. A static address map ties each software weight to its physical cell pair. This scale factor  $s$  is related to the scalar gain  $\kappa$  introduced during on-chip MAC operations to map the read current to the perceptron logits:  $s = \kappa V_{\text{read}}$ .

**Training loop (hardware-in-the-loop).** Following an initial array read, each update step proceeds as:

1. Software inference using the current  $W$  to obtain activations/logits.
2. Gradient computation for the chosen loss: backpropagation, SFF (eq. (5)), or competitive forward (eq. (9)).
3. Gradient sparsification: entries below the threshold  $\tau$  are zeroed; for layerwise schedules, frozen layers are masked.
4. Programming sweep: for each selected synapse, apply a single sub-1 V reset pulse to the appropriate device of the differential pair (pulse on  $G^-$  for a positive gradient, on  $G^+$  for a negative gradient).
5. Verification read: re-read  $(G^+, G^-)$  to update  $W$  and log statistics.

Backpropagation models are trained layerwise from output to input (Fig. 3); forward-only models are trained layerwise from input to output using their local losses (Fig. 4).

#### **Perceptron and layerwise backpropagation-based learning algorithm**

We train either a single fully connected layer (perceptron, Fig. 2) or a two-layer multilayer perceptron (MLP, Fig. 3), both without biases. The two-layer model uses 48 hidden units with ReLU activation; both architectures use a softmax output and cross-entropy loss. No normalization is applied to inputs

or activations, except in the on-chip MAC experiments where inputs are ternarized to  $x_j \in \{-1, 0, +1\}$  to match the hardware interface.

The perceptron is trained for 20 epochs. The two-layer MLP is trained for 30 epochs in a layerwise fashion: the output layer is trained for the first 10 epochs, then frozen while the input (hidden) layer is trained for the remaining 20 epochs.

We use minibatches of size 16. A batch-size study is presented in Supplementary Note 3. When MAC is performed on-chip, gradients are computed analytically from the measured outputs; when MAC is emulated, PyTorch autograd is used.

### Supervised Forward-Forward learning rule

We summarize here the specific choices used for implementing Supervised Forward-Forward learning in the experiments. For each training example with label  $y \in \{1, \dots, C\}$ , we form positive inputs by concatenating the feature vector with the corresponding one-hot label token, and negative inputs by concatenating the same feature with a randomly chosen incorrect label token. For layer  $\ell$ , let  $h_\ell^+$  and  $h_\ell^-$  denote the activations produced by the positive and negative inputs, respectively, and let the layer “goodness” be  $g_\ell(h) = \eta_\ell \|h_\ell\|_2^2$ . All SFF experiments use  $\eta = 1$ .

The per-layer loss combines positive and negative goodness terms:

$$\mathcal{L}_\ell^{SFF} = -\frac{1}{2} [\log \sigma(g_\ell(h_\ell^+) - \eta_\ell \theta_\ell^+ N_h) + \log(1 - \sigma(g_\ell(h_\ell^-) - \eta_\ell \theta_\ell^- N_h))] \quad (3)$$

where  $\sigma$  is the logistic sigmoid,  $N_h$  is the number of neurons on the output side of layer  $\ell$  (i.e. the number of activations) and the  $\theta_\ell^\pm \in \mathbb{R}$  are determined through hyperparameter optimization. Given a minibatch  $\mathcal{B}$  of  $N_B$  positive/negative activations, the gradient with respect to the weight matrix  $W_\ell$  of layer  $\ell$  is

$$\nabla_{W_\ell} \mathcal{L}_\ell^{SFF} = \frac{1}{2N_B} \sum_{h_\ell^+, h_\ell^- \in \mathcal{B}} \left[ -\frac{h_\ell^+ \nabla_{W_\ell}(h_\ell^+)}{1 + e^{g_\ell(h_\ell^+) - \eta_\ell \theta_\ell^+ N_h}} + \frac{h_\ell^- \nabla_{W_\ell}(h_\ell^-)}{1 + e^{\eta_\ell \theta_\ell^- N_h - g_\ell(h_\ell^-)}} \right]. \quad (4)$$

Considering the Rectified Linear Unit (ReLU) as the activation function, the above gradient with respect to the weight parameter  $w_{i,j}$  in layer  $\ell$  can be expressed more simply as

$$\nabla_{i,j} = - \sum_{n=1}^{N_B} \left[ \frac{h_{n,i}^+ x_{n,j}^+}{D_n^+} - \frac{h_{n,i}^- x_{n,j}^-}{D_n^-} \right]. \quad (5)$$

where  $D_n^+ = [1 + \exp(g(h_n^+) - \eta \theta^+ N_h)] / 2N_B$  and  $D_n^- = [1 + \exp(\eta \theta^- N_h - g(h_n^-))] / 2N_B$ .

This learning rule is local: the weight update for synapse connecting two neurons depends only on the activities of the neurons to which it is connected. To implement it in hardware one only needs to store the  $D_n^\pm$ ,  $h_{n,i}^\pm$ , and  $x_{n,j}^\pm$  over the minibatch and then compute eq. (5). The memory cost is of  $N_B(2 + 2N_x + 2N_h)$  parameters, where  $N_x$  and  $N_h$  are the number of neurons on the input and output side of the layer. This cost grows linearly with the number of neurons  $N_x + N_h$  (and not number of synapses  $N_x N_h$ ), therefore the requirement in working memory is sustainable (see Discussion).

Usually, an SFF layer is followed by layer normalization, to eliminate the goodness and promote the learning of new features by subsequent SFF layers<sup>15</sup>. Here, layer normalization is not needed as our

experiments use a single SFF layer followed by a cluster-based, competitive forward head, which is trained only on the positive examples (see next section).

### Learning rule used for the reading head of SFF experiments and for competitive Forward learning

We now detail the learning rule used in our experiments for the second layer (reading head) of SFF experiments and for both layers for competitive forward learning. Following<sup>16</sup>, each layer  $\ell$  partitions its activations into class-associated clusters. As in SFF, layer goodness is defined as  $g_\ell(h) = \eta_\ell \|h_\ell\|_2^2$ . When using  $\eta = 1$ , for an example with label  $y$ , the activity of the cluster tied to  $y$  is encouraged to increase, while the activity of all other clusters is discouraged. This requires only a single forward pass (no label injection into the input).

In our competitive forward experiments, we use  $\eta = 1$  for the final layer, and  $\eta = -1$  for the first layer. When using  $\eta = -1$ , for an example with label  $y$ , the activity of all clusters not tied to  $y$  is encouraged to increase, while the activity of the cluster tied to  $y$  is discouraged.

Let  $h_\ell$  denote the activations at layer  $\ell$ ,  $Z_\ell$  a binary mask selecting the cluster corresponding to the true class (and  $(1 - Z_\ell)$  the complement),  $C$  the number of classes, and  $g_\ell(h)$  the layer “goodness”. The per-layer loss is

$$\mathcal{L}_\ell^{CF} = -\frac{1}{2} [\log \sigma(g_\ell(h_\ell Z_\ell) - \eta_\ell \theta_\ell^+) + \log(1 - \sigma(g_\ell(h_\ell(1 - Z_\ell)) - \eta_\ell \theta_\ell^-))], \quad (6)$$

where  $\sigma$  is the logistic sigmoid and  $\theta_\ell^\pm \in \mathbb{R}$  are offsets.

In hardware we found it beneficial to use a temperature-based variant in which  $\theta_\ell^\pm$  scale the sigmoid arguments (rather than shift them):

$$\mathcal{L}_\ell^{CF} = -\frac{1}{2} [\log \sigma(\theta_\ell^+ g_\ell(h_\ell Z_\ell)) + \log(1 - \sigma(\theta_\ell^- g_\ell(h_\ell(1 - Z_\ell))))]. \quad (7)$$

Given a minibatch  $\mathcal{B}$  of  $N_{\mathcal{B}}$  layer inputs, the corresponding gradient with respect to the weight matrix  $W_\ell$  of layer  $\ell$  is

$$\nabla_{W_\ell} \mathcal{L}_\ell^{CF} = \frac{1}{2N_{\mathcal{B}}} \sum_{h_\ell \in \mathcal{B}} \left[ -\frac{\theta_\ell^+ (h_\ell \odot Z_\ell) \nabla_{W_\ell}(h_\ell \odot Z_\ell)}{1 + e^{\theta_\ell^+ g_\ell(h_\ell \odot Z_\ell)}} + \frac{\theta_\ell^- (h_\ell \odot (1 - Z_\ell)) \nabla_{W_\ell}(h_\ell \odot (1 - Z_\ell))}{1 + e^{-\theta_\ell^- g_\ell(h_\ell \odot (1 - Z_\ell))}} \right], \quad (8)$$

where  $\odot$  denotes element-wise multiplication with the binary masks. This formulation preserves fast convergence and allows separate control of the positive/negative contributions via  $\theta_\ell^\pm$ . Considering the Rectified Linear Unit (ReLU) as the activation function, the above gradient of the loss with respect to the weight parameter  $w_{i,j}$  in layer  $\ell$  can be expressed more simply as

$$\nabla_{i,j} = - \sum_{n=1}^{N_{\mathcal{B}}} h_{n,i} x_{n,j} \left[ \frac{\delta(C(i) = Y_n)}{D_n^+} - \frac{\delta(C(i) \neq Y_n)}{D_n^-} \right], \quad (9)$$

where  $D_n^+ = [1 + \exp(\theta^+ g(h_n \odot Z_n))] / [2N_{\mathcal{B}} \cdot \theta^+]$  and  $D_n^- = [1 + \exp(-\theta^- g(h_n \odot (1 - Z_n)))] / [2N_{\mathcal{B}} \cdot \theta^-]$ .

$C(i)$  is the class number corresponding to the cluster of neuron  $i$ .  $\delta(C(i) = Y_n)$  is one when this

class corresponds to the true class  $Y_n$ , zero otherwise (and vice-versa for  $\delta(C(i) \neq Y_n)$ ).

As for SFF, this learning rule is local: the weight update for synapse connecting two neurons depends only on the activities of the neurons to which it is connected. To implement it in hardware one only needs to store the  $D_n^\pm$ ,  $Y_n$ ,  $h_{n,i}$ , and  $x_{n,j}$  over the minibatch and then compute eq. (9). The memory cost is  $N_B(3 + N_x + N_h)$ , where  $N_x$  and  $N_h$  are the number of neurons on the input and output side of the layer. This number grows linearly with number of neurons  $N_x + N_h$  (and not number of synapses  $N_x N_h$ ), therefore the requirement in working memory is sustainable (see Discussion), and lower than for SFF.

### Statistical analysis of the experimental results

The final test accuracies for the two-layer perceptron trained with backpropagation are 90.62%, 91.18%, 89.89%, 87.87%, 90.44%. For SFF, the accuracies are 88.05%, 90.44%, 87.68%, 89.89%, 91.36%. For competitive forward, the accuracies are 91.18%, 90.62%, 89.52%, 90.44%, 86.03%. We tested pairwise null hypotheses of equal means:  $H_0^{\text{bp-sff}} : \mu_{\text{bp}} = \mu_{\text{sff}}$ ,  $H_0^{\text{bp-cf}} : \mu_{\text{bp}} = \mu_{\text{cf}}$ ,  $H_0^{\text{sff-cf}} : \mu_{\text{sff}} = \mu_{\text{cf}}$ ; where  $\mu_x$  is the averaged final accuracies for the learning rule  $x$ . By computing a two-tailed Welch's t-test, we get  $p^{\text{bp-sff}} = 0.586$ ,  $p^{\text{bp-cf}} = 0.697$ ,  $p^{\text{sff-cf}} = 0.951$ . All p-values largely exceed  $\alpha = 0.05$ . The conclusion is unchanged after Holm-Bonferroni correction.

### Energy consumption analysis of the learning process

During training we logged, for every reset event, the device address and the conductance  $G$  measured immediately before. The energy delivered to a memristor during a single reset pulse was estimated as  $E_{\text{pulse}} = GV_{\text{reset}}^2 t_{\text{reset}}$ , where  $V_{\text{reset}}$  and  $t_{\text{reset}}$  are the pulse voltage and duration used for sub-1 V reset (see Suppl. Note 2). The total programming energy for a run is the sum of  $E_{\text{pulse}}$  over all pulses applied to the active device of each differential pair.

To project the programming energy with the lower-voltage (MAC-array) device technology, we recomputed  $E_{\text{pulse}}$  for the exact sequence of pulses recorded on the Large Array but substituting the MAC-array pulse parameters (Suppl. Note 2). For the program-and-verify baseline, we used its prescribed program pulses and verify reads (amplitudes, widths) from a prior work using hafnium oxide memristors<sup>9</sup>; the reported baseline energy includes the mean number of attempts and verify reads until the target criterion is met reported in this work.

For array reads (vector-matrix products), energy is dominated in our experimental setup by the read pulse due to the relatively long integration time. We therefore estimate the read energy by summing the read pulse energy over all forward passes that need to be executed during training (one pass per layer for competitive forward; two passes for SFF). By contrast, in a fully integrated CMOS implementation with short read pulses, peripheral circuits (e.g., ADCs) dominate energy. To estimate a realistic end-to-end MAC cost (including ADC), we use the measured energy efficiency of a state-of-the-art foundry in-memory-computing platform in 22 nm using memristors<sup>34</sup>. For the precision closest to our use case (4-bit weights, 2-bit input activations, 10-bit outputs), the reported efficiency in<sup>34</sup> is 57.5 TOPS/W. We convert the total number of MAC operations executed during training (note that in this context, one MAC is counted as two operations: one multiply plus one add).

## Computer setup

All hardware experiments were orchestrated from a workstation equipped with an Intel Xeon E5-2640 CPU. Control software was written in Python 3.11 using the PyTorch 2.7 framework and handled coordination of the WGFMU and microcontroller, dataset handling, and training loops. All simulations reported in the Supplementary Notes were executed on a server with a NVIDIA GeForce RTX 2080 Ti (11 GB VRAM). These simulations were implemented in Python 3.9 using the JAX and JAXLIB 0.4 framework.

## References

1. Kim, H., Mahmoodi, M., Nili, H. & Strukov, D. B. 4k-memristor analog-grade passive crossbar circuit. *Nat. communications* **12**, 5198 (2021).
2. Wan, W., Kubendran, R., Schaefer, C., Eryilmaz, S. B., Zhang, W., Wu, D., Deiss, S., Raina, P., Qian, H., Gao, B. *et al.* A compute-in-memory chip based on resistive random-access memory. *Nature* **608**, 504–512 (2022).
3. Hung, J.-M., Xue, C.-X., Kao, H.-Y., Huang, Y.-H., Chang, F.-C., Huang, S.-P., Liu, T.-W., Jhang, C.-J., Su, C.-I., Khwa, W.-S. *et al.* A four-megabit compute-in-memory macro with eight-bit precision based on cmos and resistive random-access memory for ai edge devices. *Nat. Electron.* **4**, 921–930 (2021).
4. Huang, Y., Ando, T., Sebastian, A., Chang, M.-F., Yang, J. J. & Xia, Q. Memristor-based hardware accelerators for artificial intelligence. *Nat. Rev. Electr. Eng.* 1–14 (2024).
5. Li, C., Ignowski, J., Sheng, X., Wessel, R., Jaffe, B., Ingemi, J., Graves, C. & Strachan, J. P. Cmos-integrated nanoscale memristive crossbars for cnn and optimization acceleration. In *2020 IEEE International Memory Workshop (IMW)*, 1–4 (IEEE, 2020).
6. Yousuf, O., Hoskins, B. D., Ramu, K., Fream, M., Borders, W. A., Madhavan, A., Daniels, M. W., Dienstfrey, A., McClelland, J. J., Lueker-Boden, M. *et al.* Layer ensemble averaging for fault tolerance in memristive neural networks. *Nat. Commun.* **16**, 1250 (2025).
7. Ambrogio, S., Narayanan, P., Okazaki, A., Fasoli, A., Mackin, C., Hosokawa, K., Nomura, A., Yasuda, T., Chen, A., Friz, A. *et al.* An analog-ai chip for energy-efficient speech recognition and transcription. *Nature* **620**, 768–775 (2023).
8. Le Gallo, M., Khaddam-Aljameh, R., Stanisavljevic, M., Vasilopoulos, A., Kersting, B., Dazzi, M., Karunaratne, G., Brändli, M., Singh, A., Mueller, S. M. *et al.* A 64-core mixed-signal in-memory compute chip based on phase-change memory for deep neural network inference. *Nat. Electron.* **6**, 680–693 (2023).
9. Esmanhotto, E., Hirtzlin, T., Bonnet, D., Castellani, N., Portal, J.-M., Querlioz, D. & Vianello, E. Experimental demonstration of multilevel resistive random access memory programming for up to two months stable neural networks inference accuracy. *Adv. Intell. Syst.* **4**, 2200145 (2022).
10. Rao, M., Tang, H., Wu, J., Song, W., Zhang, M., Yin, W., Zhuo, Y., Kiani, F., Chen, B., Jiang, X. *et al.* Thousands of conductance levels in memristors integrated on cmos. *Nature* **615**, 823–829 (2023).

11. Stecconi, T., Guido, R., Berchialla, L., La Porta, A., Weiss, J., Popoff, Y., Halter, M., Sousa, M., Horst, F., Dávila, D. *et al.* Filamentary taox/hfo2 rram devices for neural networks training with analog in-memory computing. *Adv. electronic materials* **8**, 2200448 (2022).
12. Park, J., Kumar, A., Zhou, Y., Oh, S., Kim, J.-H., Shi, Y., Jain, S., Hota, G., Qiu, E., Nagle, A. L. *et al.* Multi-level, forming and filament free, bulk switching trilayer rram for neuromorphic computing at the edge. *Nat. Commun.* **15**, 3492 (2024).
13. Wen, T.-H., Hung, J.-M., Huang, W.-H., Jhang, C.-J., Lo, Y.-C., Hsu, H.-H., Ke, Z.-E., Chen, Y.-C., Chin, Y.-H., Su, C.-I. *et al.* Fusion of memristor and digital compute-in-memory processing for energy-efficient edge computing. *Science* **384**, 325–332 (2024).
14. Martemucci, M., Rummens, F., Malot, Y., Hirtzlin, T., Guille, O., Martin, S., Carabasse, C., Vincent, A. F., Saïghi, S., Grenouillet, L. *et al.* A ferroelectric-memristor memory for both training and inference. *Nat. Electron.* 1–13 (2025).
15. Hinton, G. The forward-forward algorithm: Some preliminary investigations. *arXiv preprint arXiv:2212.13345* **2**, 5 (2022).
16. Papachristodoulou, A., Kyrkou, C., Timotheou, S. & Theocharides, T. Convolutional channel-wise competitive learning for the forward-forward algorithm. AAAI'24/IAAI'24/EAAI'24, DOI: [10.1609/aaai.v38i13.29369](https://doi.org/10.1609/aaai.v38i13.29369) (AAAI Press, 2024).
17. Lin, Y.-P., Bennett, C. H., Cabaret, T., Vodenicarevic, D., Chabi, D., Querlioz, D., Jousselme, B., Derycke, V. & Klein, J.-O. Physical realization of a supervised learning system built with organic memristive synapses. *Sci. reports* **6**, 31932 (2016).
18. Alibart, F., Zamanidoost, E. & Strukov, D. B. Pattern classification by memristive crossbar circuits using ex situ and in situ training. *Nat. communications* **4**, 2072 (2013).
19. Prezioso, M., Merrikh-Bayat, F., Hoskins, B., Adam, G. C., Likharev, K. K. & Strukov, D. B. Training and operation of an integrated neuromorphic network based on metal-oxide memristors. *Nature* **521**, 61 (2015).
20. Serb, A., Bill, J., Khiat, A., Berdan, R., Legenstein, R. & Prodromakis, T. Unsupervised learning in probabilistic neural networks with multi-state metal-oxide memristive synapses. *Nat. communications* **7**, 12611 (2016).
21. Zhang, W., Yao, P., Gao, B., Liu, Q., Wu, D., Zhang, Q., Li, Y., Qin, Q., Li, J., Zhu, Z. *et al.* Edge learning using a fully integrated neuro-inspired memristor chip. *Science* **381**, 1205–1211 (2023).
22. Li, C., Belkin, D., Li, Y., Yan, P., Hu, M., Ge, N., Jiang, H., Montgomery, E., Lin, P., Wang, Z. *et al.* Efficient and self-adaptive in-situ learning in multilayer memristor neural networks. *Nat. communications* **9**, 2385 (2018).
23. Yi, S.-i., Kendall, J. D., Williams, R. S. & Kumar, S. Activity-difference training of deep neural networks using memristor crossbars. *Nat. Electron.* **6**, 45–51 (2023).
24. Van Doremaele, E. R., Stevens, T., Ringeling, S., Spolaor, S., Fattori, M. & van de Burgt, Y. Hardware implementation of backpropagation using progressive gradient descent for in situ training of multilayer neural networks. *Sci. Adv.* **10**, eado8999 (2024).

25. Imbert, B., Renaudineau, A., Diallo, M., Aguirre-Morales, J.-D., Iftakher, M., Harabi, K.-E., Turck, C., Drouhin, M., Hirtzlin, T., Vianello, E. *et al.* Forward-forward learning exploiting low-voltage reset of rram. In *2024 IEEE International Electron Devices Meeting (IEDM)*, 1–4 (IEEE, 2024).
26. Pallo, M., D'Agostino, S., Piccoli, M., Bonnet, D., Castellani, N., Piccolboni, G., Iftakher, M., Nodin, J.-F., Andrieu, F., Querlioz, D. *et al.* On chip customized learning on resistive memory technology for secure edge ai. In *2025 Symposium on VLSI Technology and Circuits (VLSI Technology and Circuits)*, 1–3 (IEEE, 2025).
27. Baroni, A., Glukhov, A., Perez, E., Wenger, C., Ielmini, D., Olivo, P. & Zambelli, C. Low conductance state drift characterization and mitigation in resistive switching memories (rram) for artificial neural networks. *IEEE Transactions on Device Mater. Reliab.* **22**, 340–347 (2022).
28. Majumdar, A., Bocquet, M., Hirtzlin, T., Laborieux, A., Klein, J.-O., Nowak, E., Vianello, E., Portal, J.-M. & Querlioz, D. Model of the weak reset process in hfo x resistive memory for deep learning frameworks. *IEEE Transactions on Electron Devices* **68**, 4925–4932 (2021).
29. Miro-Panades, I., Lorrain, V., Billod, L., Kucher, I., Templier, V., Choisnet, S., Ali, N., Rossigneux, B., Bichler, O. & Valentian, A. A  $772\mu\text{J}/\text{frame}$  imangenet feature extractor accelerator on hd images at 30fps. In *2024 IEEE Asia Pacific Conference on Circuits and Systems (APCCAS)*, 25–29 (IEEE, 2024).
30. Chen, Y., Yin, G., Tan, Z., Lee, M., Yang, Z., Liu, Y., Yang, H., Ma, K. & Li, X. Yoloc: Deploy large-scale neural network by rom-based computing-in-memory using residual branch on a chip. In *Proceedings of the 59th ACM/IEEE Design Automation Conference*, 1093–1098 (2022).
31. Yin, G., Chen, Y., Zhou, M., Tang, W., Lee, M., Yang, Z., Liao, T., Du, X., Narayanan, V., Yang, H. *et al.* Cramming more weight data onto compute-in-memory macros for high task-level energy efficiency using custom rom with 3984-kb/mm<sup>2</sup> density in 65-nm cmos. *IEEE J. Solid-State Circuits* **59**, 1912–1925 (2023).
32. Yu, T., Chen, Z., Chen, Y., Wang, S., Liu, Y., Yang, H. & Li, X. Dsc-rom: A fully digital sparsity-compressed compute-in-rom architecture for on-chip deployment of large-scale dnns. In *2025 Design, Automation & Test in Europe Conference (DATE)*, 1–6 (IEEE, 2025).
33. Jebali, F., Majumdar, A., Turck, C., Harabi, K.-E., Faye, M.-C., Muhr, E., Walder, J.-P., Bilousov, O., Michaud, A., Vianello, E. *et al.* Powering ai at the edge: A robust, memristor-based binarized neural network with near-memory computing and miniaturized solar cell. *Nat. Commun.* **15**, 741 (2024).
34. Xue, C.-X., Chiu, Y.-C., Liu, T.-W., Huang, T.-Y., Liu, J.-S., Chang, T.-W., Kao, H.-Y., Wang, J.-H., Wei, S.-Y., Lee, C.-Y. *et al.* A cmos-integrated compute-in-memory macro based on resistive random-access memory for ai edge devices. *Nat. Electron.* **4**, 81–90 (2021).
35. Hiratani, N. & Fukai, T. Redundancy in synaptic connections enables neurons to learn optimally. *Proc. Natl. Acad. Sci.* **115**, E6871–E6879, DOI: [10.1073/pnas.1803274115](https://doi.org/10.1073/pnas.1803274115) (2018). <https://www.pnas.org/doi/pdf/10.1073/pnas.1803274115>.

36. Bernstein, J., Wang, Y.-X., Azizzadenesheli, K. & Anandkumar, A. signs gd: Compressed optimisation for non-convex problems. In *International conference on machine learning*, 560–569 (PMLR, 2018).
37. Bernstein, J. & Newhouse, L. Old optimizer, new norm: An anthology. *arXiv preprint arXiv:2409.20325* (2024).
38. Balles, L., Pedregosa, F. & Roux, N. L. The geometry of sign gradient descent. *arXiv preprint arXiv:2002.08056* (2020).
39. Harabi, K.-E., Hirtzlin, T., Turck, C., Vianello, E., Laurent, R., Droulez, J., Bessière, P., Portal, J.-M., Bocquet, M. & Querlioz, D. A memristor-based bayesian machine. *Nat. Electron.* **6**, 52–63 (2023).
40. Bonnet, D., Hirtzlin, T., Majumdar, A., Dalgalty, T., Esmanhotto, E., Meli, V., Castellani, N., Martin, S., Nodin, J.-F., Bourgeois, G. *et al.* Bringing uncertainty quantification to the extreme-edge with memristor-based bayesian neural networks. *Nat. Commun.* **14**, 7530 (2023).
41. Harabi, K.-E., Turck, C., Drouhin, M., Renaudineau, A., Bersani-Veroni, T., Querlioz, D., Hirtzlin, T., Vianello, E., Bocquet, M. & Portal, J.-M. A multimode hybrid memristor-cmos prototyping platform supporting digital and analog projects. In *Proceedings of the 28th Asia and South Pacific Design Automation Conference*, 184–185 (2023).
42. Russakovsky, O., Deng, J., Su, H., Krause, J., Satheesh, S., Ma, S., Huang, Z., Karpathy, A., Khosla, A., Bernstein, M. *et al.* Imagenet large scale visual recognition challenge. *Int. journal computer vision* **115**, 211–252 (2015).